Diaminocarbenes; Calculation of Barriers to Rotation about $C_{carbene}$−N Bonds, Barriers to Dimerization, Proton Affinities, and ^{13}C NMR Shifts

Roger W. Alder* and Michael E. Blake

School of Chemistry, University of Bristol, Bristol BS8 1TS, U.K.

Josep M. Oliva*

Institut de Ciència de Materials de Barcelona, CSIC, Campus de la UAB, Bellaterra E-08193, Spain

Received: September 24, 1999

Barriers to rotation about the $C_{carbene}$−N bonds in diaminocarbene $(H_2N)_2C$ **1a**, bis(dimethylamino)carbene $((CH_3)_2N)_2C$ **1b**, the related formamidinium ions $(H_2N)_2CH^+$ **2a** and $((CH_3)_2N)_2CH^+$ **2b**, and the Li^+ complexes $(H_2N)_2CLi^+$ **3a** and $((CH_3)_2N)_2CLi^+$ **3b** have been calculated using density-functional theory in order to study the extent of π-bond stabilization of the carbene center. Experimental barriers from DNMR are reported for **1b** and **2b** and compared with those for bis(diisopropylamino)carbene **1c** and the *N*,*N*,*N*′,*N*′-tetraisopropylformamidinium ion **2c**; rotational barriers computed for **1b** and **2b** including thermal corrections compare well with experiment. The dimerization of **1a** and **1b** have been studied with (full) geometry optimization up to the levels QCISD(T)/cc-pVDZ//MP2/cc-pVDZ and B3LYP/cc-pVDZ//B3LYP/cc-pVDZ, respectively. The minimum-energy path for the dimerization of **1a** has been computed using the BPW91/cc-pVDZ method. It is shown that the transition state geometries for the dimerizations of **1a** and **1b** have C_2 and C_1 symmetry, respectively, the latter being strongly polarized. The possible involvement of catalysis by protons and lithium ions in the dimerization processes is discussed. Calculations of the proton affinities of **1a**, **1b**, and some related species are reported. ^{13}C NMR shielding constant calculations on a series of diaminocarbenes have been performed using the gauge-including atomic orbitals (GIAO) method. The variation in the extremely downfield-shifted ^{13}C NMR signal of the carbene carbon in **1a**, **1b**, and related species is reproduced reasonably well by GIAO calculations, the latter being 2−8 ppm more upfield than the experimentally observed signals. It is shown that the paramagnetic contributions to the shielding tensor at the carbene nucleus play an important role in the chemical shift changes upon substitution in the $RXC(NR_2)$ species.

Introduction

Since the first observation of an imidazol-2-ylidene by the Arduengo group in1991,[1] a widening range of diaminocarbenes have been observed,[2,3] including the first air stable carbene, **4a**.[4] Aromatic imidazol-2-ylidenes are thermodynamically stable to dimerization,[5,6] but dihydroimidazol-2-ylidenes[7,8] and acyclic diaminocarbenes with appropriate steric hindrance, like bis(diisopropylamino)carbene **1c**,[9] can also be isolated. Most of these carbenes have been prepared by deprotonation of imidazolium or amidinium salts, but desulfurization of thioureas by potassium,[10] and thermolysis of methanol adducts[11] have also been used. Stable carbenes with adjacent heteroatoms other than nitrogen are restricted to the unique phosphinocarbenes,[12,13] e.g., **5**, an aromatic thiazol-2-ylidene,[14] **6**, related to the thiamine intermediate.[15] Warkentin has made important studies of aminooxy- and dialkoxycarbenes,[16,17] and several stable aminooxy- and aminothiocarbenes, e.g., **7a** and **7b**, have been generated in our laboratories.[18]

Unhindered diaminocarbenes such as bis(dimethylamino)carbene **1b**,[19] 1,3-dimethyl-2-imidazolidinylidene **8**,[8] and bis(*N*-piperidinyl)carbene **9** dimerize remarkably slowly at ambient temperatures. In most cases these carbenes have been generated by deprotonation of amidinium salts with lithium amide bases, and it has been shown that complexation with lithium, sodium, and even potassium species can occur, and that this probably affects the rate of dimerization.[20,21]

The dimerization of singlet methylene has been extensively examined theoretically, following the original suggestion by Hoffmann, Gleiter, and Mallory[22] that this reaction cannot proceed by a least motion pathway. The most recent major study[23] suggested a barrier of about 170 kJ mol^{-1} for the nonleast motion process and moreover that it led to a Rydberg excited state of ethene. In this paper, we discuss the dimerization of **1a** and **1b**, models for systems that can be studied experimentally.

An important question concerning species such as **1** is the extent of π-bond stabilization of the carbene center. Experimentally, this can be studied for carbenes where the X−$C_{carbene}$−N unit is not part of a ring by measurement of the barrier to rotation about the $C_{carbene}$−N bond, and results have been obtained[9,18] for **1c** and **7a**. We have therefore studied this rotation process computationally for **1a** and **1b**, for the corresponding protonated ions $(H_2N)_2CH^+$ **2a** and $((CH_3)_2N)_2CH^+$ **2b**, and for their Li^+ complexes $(H_2N)_2CLi^+$ **3a** and $((CH_3)_2N)_2CLi^+$ **3b**.

Diaminocarbenes such as **1b** and **1c**, imidazol-2-ylidenes (e.g., **4a**), and related species such as **6** and **7** have been generated by deprotonation, and it is therefore interesting to enquire what the pK_a of the corresponding protonated ions is. We have

* To whom correspondence should be addressed. E-mail for R.W.A.: rog.alder@bristol.ac.uk. E-mail for J.M.O.: oliva@icmab.es.

10.1021/jp9934228 CCC: $18.00
Published on Web 12/01/1999

reported the pK_a of the conjugate acid of imidazol-2-ylidene **4b** in DMSO,[24] and proton affinities (PA) have been calculated for the parent imidazol-2-ylidene **4c**[25] and for some simpler carbenes,[26] of which the most relevant was $C(OH)_2$.[27] Accordingly we have calculated the PA values for **1a** and **1b** and **4c**. B3LYP/6-31G* calculations on imidazol-2-ylidenes have also been performed by Muchall et al.[28]

Finally, one of the outstanding characteristics of these carbenes is the extreme downfield shift of the $C_{carbene}$ in the ^{13}C NMR spectrum. Experimental shifts between 200 and 300 ppm downfield from TMS have now been observed, and some structural trends within this range are now becoming apparent. We have therefore performed gauge-including atomic orbitals (GIAO) calculations of the shifts for **1a**, **1b**, and some related species. The chemical shift tensor for one stable carbene has been published,[29] and some calculations by a density-functional theory (DFT)-hybrid GIAO method on the chemical shift tensors of related silylenes have been recently reported.[30]

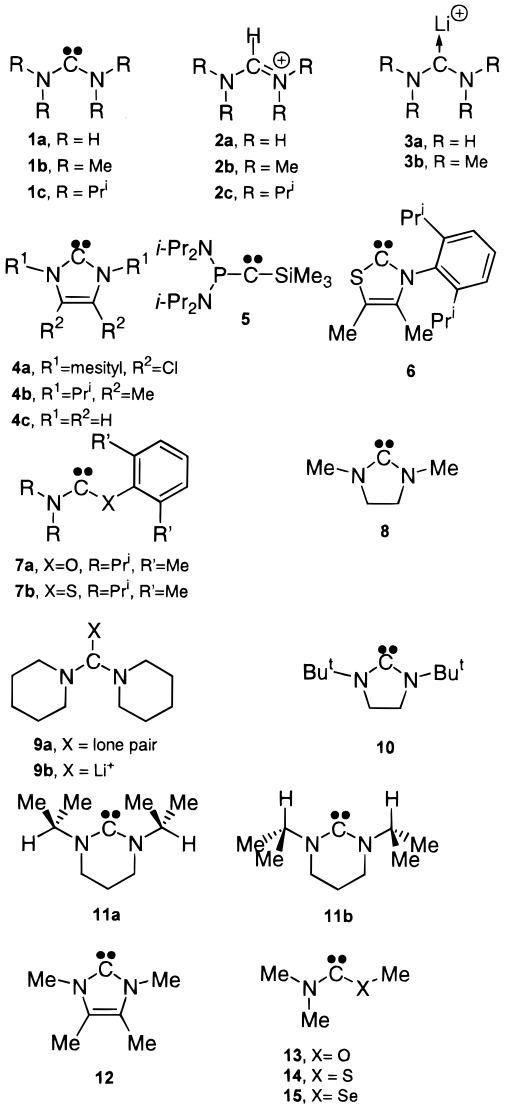

Experimental and Computational Procedures

1. Determination of Rotational Barriers. All solvents were anhydrous, and all manipulations where performed under a nitrogen atmosphere. Filtrations were performed using a sintered filter stick.

Purification of N,N,N′,N′-Tetramethylformamidinium Chloride. The commercially available salt (Aldrich) was carefully recrystallized and dried before use.

N,N,N′,N′-Tetramethylformamidinium Trifluoromethanesulfonate. Methyl trifluoromethanesulfonate (1.0 mL, 8.84 mmol) was added to a dichloromethane solution (4 mL; −78 °C) of tetramethylformamidinium chloride (0.585 g, 4.29 mmol) under nitrogen. This was allowed to stir at room temperature for 30 min before the volatile fractions were removed by application of a high vacuum, giving a purple solid. This solid was heated gently in anhydrous diethyl ether (10 mL) and then sonicated for 5 min. The purple supernatant liquid was discarded into methanolic potassium hydroxide. This process was repeated until no purple color persisted. The salt was then dried by slow application of a high vacuum at 0 °C to yield the hygroscopic salt (1.06 g, 99%) as a white powder, d_H(300 MHz; CD_3CN) 3.15 (6 H, s, CH_3), 3.24 (6 H, s, CH_3), and 7.48 (1 H, s, (C2)H); d_C(75 MHz; $CDCl_3$) 35.4 (CH_3), 46.2 (CH_3), 120.8 (q, J 319, $-CF_3$), and 156.9 (C2). This salt may alternatively be prepared by reaction of the chloride salt with silver triflate.

Preparation of a Solution of Bis(dimethylamino)carbene in THF-d_8. *n*-Butyllithium (2.6 equiv, ca. 2.5 M in hexanes, recently titrated and containing no more than 0.1 M LiOH) was reduced to a viscous oil by applying a high vacuum while raising the temperature from −78 °C to ambient to remove the solvent. This oil was cooled to −78 °C and deuterated solvent THF-d_8 (0.4 mL) added. *N,N,N′,N′*-Tetramethylpiperidine (1.2 equiv) was added to this solution, and the reaction mixture was allowed to warm to room temperature. The resulting lithium amide was then added to tetramethylformamidinium chloride (150 mg) suspended in the deuterated solvent (0.4 mL; −78 °C), and the solution was allowed to warm to room temperature.

Dynamic NMR Measurements. All data were acquired on a JEOL GX400 spectrometer operating at 400 MHz. Temperatures were calibrated by the usual methanol thermometer.[31] Warming and cooling were done slowly in 10 °C intervals, allowing 10 min for equilibration at each stage before a ^1H NMR spectrum was acquired. Near the coalescence temperature, the temperature was stepped in 1 °C intervals. Coalescence was deemed to have occurred when a flat plateau was obtained between the two merging peaks.

The coalescence temperature (T_c) for *N,N,N′,N′*-tetramethylformamidinium trifluoromethanesulfonate (28 mg, 0.112 mmol) in THF-d_8 (0.723 g) was determined as 38 °C from a peak separation ($\Delta\nu$) of 40 Hz, giving a rotation barrier ($\Delta G_c^{\ddagger}$) of 64.6 kJ mol^{-1}. The peak separation ($\Delta\nu$) for this salt was strongly temperature-dependent, and so $\Delta\nu$ at T_c (38 °C) was determined by extrapolation of the peak separation from −90 to 0 °C.

The temperature of coalescence for bis(dimethylamino)-carbene in THF-d_8 (T_c) was measured as −51 °C with a peak separation ($\Delta\nu$) of 117 Hz, giving a rotation barrier ($\Delta G_c^{\ddagger}$) of 43.5 kJ mol^{-1}.

2. Theoretical Methods. All calculations in this work were performed using the suite of programs Gaussian94, Revision E.1[32] with Pople's 6-31G* and Dunning's correlation consistent cc-pVDZ basis sets, respectively.[33] Computations in compounds **1a**, **1b**, **2a**, **2b**, **3a**, and **3b** were carried out using the B3LYP/6-31G*//B3LYP/6-31G* model. In the dimerization of **1a**, complete active-space self-consistent field (CASSCF), second-order Møller−Plesset perturbation (MP2), density-functional theory (DFT, with the B3LYP and BPW91 functionals[34]), and QCISD(T) approaches were used. Owing to the larger size of **1b**, only the DFT methods were used in the calculation of stationary points for its dimerization. The ^{13}C NMR shielding

TABLE 1: Optimized Geometries for the C_{2v} Singlet/C_2 Triplet 1a and C_2 Singlet/C_2 Triplet 1b[a]

	singlet			triplet			
method/basis set	R_{CN}	α	γ	R_{CN}	α	γ	ΔE(S − T)
			1a				
(U)MP2/6-31G*	1.346	111.5	0	1.396	121.9	11.3	220.6
(U)MP2/cc-pVDZ	1.347	111.6	0	1.402	122.0	28.7	220.5
BPW91/6-31G*	1.349	112.2	0	1.397	121.9	10.4	211.1
BPW91/cc-pVDZ	1.347	112.6	0	1.397	122.0	23.2	213.5
B3LYP/6-31G*	1.344	112.2	0	1.393	122.2	22.7	217.8
B3LYP/cc-pVDZ	1.341	112.5	0	1.393	122.3	25.0	220.9
			1b				
(U)MP2/6-31G*	1.357	117.1	1.3	1.390	121.2	16.2	185.2
BPW91/6-31G*	1.361	119.8	0.2	1.393	121.3	12.7	168.5
BPW91/cc-pVDZ	1.360	120.3	0.2	1.393	121.2	12.1	169.0
B3LYP/6-31G*	1.354	119.7	0.3	1.389	121.8	12.7	172.9
B3LYP/cc-pVDZ	1.354	120.0	0.4	1.388	121.6	12.3	173.4

[a] See Figure 2 for definition of geometry parameters; $\gamma = 360 - (\beta_1 + \beta_2 + \beta_3)$ is the pyramidalization angle on nitrogen. Distances in Ångstrom, angles in degrees. (U)MP2 correspond to (triplet)singlet calculations. ΔE(S − T) is the singlet−triplet splitting in kJ mol^{-1}, at $T = 0$ K and without zero-point energy corrections.

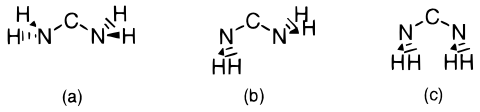

Figure 1.

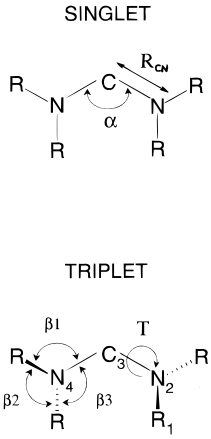

Figure 2. Geometrical parameters in the singlet and triplet diaminocarbenes **1a** (R = H) and **1b** (R = CH_3). R_{CN} and α are the $C_{carbene}$−N distance and ∠$NC_{carbene}$N angle, respectively. The pyramidalization on nitrogen is measured as $\gamma = 360 - (\beta_1 + \beta_2 + \beta_3)$: $\gamma = 0$ indicates a planar nitrogen; the larger γ, the more pyramidalized the nitrogen. T is the torsional angle $R_1N_2-C_3N_4$.

tensors for compounds **1**, **2**, **4**, and **9**−**15** were computed using the gauge-including atomic orbitals (GIAO) approach.[35] The calculated ^{13}C shifts were calibrated with respect to (a) TMS as well as (b) Forsyth's equation.[55]

Results and Discussion

A. Electronic Structure. In this section we will be concerned with the geometries, electronic configuration, and singlet−triplet (S−T) energy gaps in diaminocarbene **1a** and bis(dimethylamino)carbene **1b**.

Table 1 and Figure 2 show the geometries, energies, and S−T energy gaps for **1a** and **1b** in their singlet and triplet states. The singlet stability in these species stems from the π-donor, σ-acceptor nature of the amino substituents thereby efficiently withdrawing excess σ-electron density from the $C_{carbene}$ center and diminishing its π-electron deficiency via $p_\pi-p_\pi$ back-donation from the nitrogen lone pairs. Consequently, singlet **1a** is planar (C_{2v} symmetry), and singlet **1b** is close to planar (C_2 symmetry, with ∼1° of pyramidalization on nitrogens).

As shown in Table 1, the C−N distance and ∠NCN angle in singlet and triplet **1a** are relatively insensitive to the calculational level. The C−N distance in singlet **1a** is significantly shorter than that expected for an sp^2-sp^2 C−N bond length in a case where there is no π-overlap although it is obviously longer than that for a C═N double bond (a B3LYP/6-31G* geometry optimization on $H_2C{=}N-CH{=}CH_2$ with a C−N−C−C torsional angle constrained to 90° gives R(C═N) = 1.268 Å and R(N−C) = 1.410 Å).[36] The partial π-bonding is discussed later in connection with rotational barriers. The C−N distance is elongated in triplet **1a** owing to the electronic repulsion between the $2p_\pi$ electron and the electrons in the nitrogen lone pairs, and the geometry at the nitrogen atoms becomes pyramidal. These changes further support partial π-bonding in the singlet. The ∠NCN angle opens up ∼10°, and the molecule loses its C_{2v} planarity for C_2 nonplanar symmetry. Heinemann and Thiel[37] reported that triplet **1a** had nonplanar C_{2v} symmetry. The preferred conformation of the triplet **1a** has the nitrogen lone pairs "in, in" (Figure 1a) rather than "in, out" or "out, out" (Figure 1b,c).[38] Similar geometrical trends were found for **1b** as for **1a** (Table 1), the main difference being the nonplanarity of the singlet in **1b** (C_2 symmetry). The pyramidalization on nitrogens is barely 2°, and therefore, apart from the hydrogens in the methyl groups, the species is almost planar. In the singlet, the slightly larger C−N distance (by ∼0.01 Å) and ∠NCN angle (by ∼6°) in **1b** as compared to **1a** can be attributed to steric effects of the methyl groups. In the triplet **1b** the $C_{carbene}$−N distance and ∠$NC_{carbene}$N angle show analogous trends as compared to **1a**.

It is well-known that (apart from being very reactive) the methylene molecule CH_2 is a triplet in its ground state, the T−S gap being ∼40 kJ mol^{-1}. Heinemann and Thiel[37] reported a S−T gap for **1a** of 245 kJ mol^{-1} using an MP2/TZ2P//HF/TZ2P wave function. As shown in Table 1 the S−T gaps for **1a** and **1b** are, respectively, 221 and 173 kJ mol^{-1} (B3LYP/cc-pVDZ model), reversed in sign and about 4−5 times larger than in CH_2. Carbene **1a** has been observed in neutralization−reionization mass spectrometric (NRMS) experiments,[39] by one-electron reduction of its corresponding radical cation. According to McGibbon et al.,[39] the relatively small S−T gap and the limited number of potential precursors make the prospects for generating **1a** as persistent species in the condensed phase slim.[40] However, in our opinion, a more important point is that **1a** is expected to undergo rapid intermolecular proton transfers in solution to give formamidine, $H_2N-CH{=}NH$, a much more stable species. This is not a problem for **1b**, as shown by its detection in solution by Alder and Blake.[19]

B. Rotational Barriers about $C_{carbene}$−N. The π-bond stabilization of the $C_{carbene}$ center in a diaminocarbene is closely related to the barrier to rotation about the $C_{carbene}$−N bond, as mentioned in the Introduction. Barriers to rotation have been measured using dynamic ^{1}H NMR techniques for carbene **1c** ($\Delta G^\ddagger$ = 53 kJ mol^{-1}, coalescence temperature $T_c = -10$ °C), and its formamidinium ion **2c** ($\Delta G^\ddagger$ = 55 kJ mol^{-1}, T_c = 8 °C), and lower limits have been put on the barrier for the aminooxycarbene **7a** ($\Delta G^\ddagger$ = 88 kJ mol^{-1}, T_c > 105 °C).[9,18] A barrier for rotation in **2b** with an unusual organometallic counterion has been reported,[41] but we report the barriers for **1b** and for **2b**·CF_3SO_3 under the same conditions in THF.

Figure 3 and Table 2 show, respectively, the parameters and optimized geometries for the protonated and Li^+ complexed ions **2a**, **2b**, **3a**, and **3b**, and for the transition states for the process of rotation about the $C_{carbene}$−N bond in species **1a**, **1b**, **2a**, **2b**, **3a**, and **3b** using the B3LYP/6-31G* model. In Table 2, r, R_{rot},

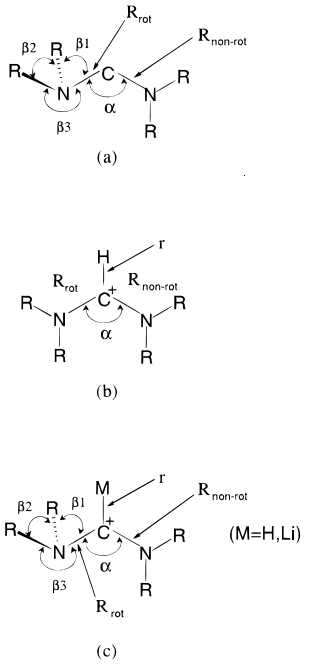

Figure 3. Reactant and transitions state (TS) geometrical parameters in the rotation of $\angle NR_2$ about the $C_{carbene}-N$ bond. (a) R = (H,Me) → (**1a**-TS, **1b**-TS). (b) R = (H, Me) → (**2a**, **2b**). (c) M = H, R = (H, Me) → (**2a**-TS, **2b**-TS); M = Li, R = (H, Me) → (**3a**-TS, **3b**-TS). *r*, R_{rot}, and $R_{non-rot}$ are the (H, M)$-C_{carbene}$, $C_{carbene}-N$ (rotation), and $C_{carbene}-N$ (no rotation) bond distances, and α is the $\angle NC_{carbene}N$ angle. The pyramidalization on nitrogen is defined as in Figure 2.

TABLE 2: Optimized Geometries of Reactant and Transition State (TS) and Energy Barriers (kJ mol^{-1}) for Rotation about the $C_{carbene}-N$ Bond in 1a, 2a, 3a, 1b, 2b, and 3b[a]

species	*r*	R_{rot}	$R_{non-rot}$	α	*γ*	Δ*E*
1a-TS		1.480	1.316	105.2	50.1	82.9
2a	1.086	1.314	1.314	125.4	0.0	
2a-TS	1.096	1.388	1.287	118.3	31.3	110.6
3a	2.088	1.335	1.335	115.5	0.0	
3a-TS	2.097	1.444	1.302	108.4	35.9	101.3
1b-TS		1.469	1.323	110.6	35.6	45.9
2b	1.086	1.324	1.324	131.0	12.6	
2b-TS	1.098	1.387	1.294	122.8	26.5	75.5
3b	2.067	1.346	1.346	121.0	0.7	
3b-TS	2.000	1.469	1.323	110.6	35.6	62.4

[a] Calculations with the B3LYP/6-31G* model. See Figure 3 for definition of geometry parameters. All calculations correspond to the species at $T = 0$ K without zero-point energy corrections.

and $R_{non-rot}$ correspond, respectively, to the distance between the cation (H^+ and Li^+) and the $C_{carbene}$ center, the $C_{carbene}-N$ distance in the bond where rotation occurs, and the other $C_{carbene}-N$ distance; α is the $\angle NC_{carbene}N$ angle. In all species, R_{rot} is elongated as the TS is reached owing to the loss of π-bonding. The larger increase for the carbene and lithium complex series may be due to repulsion between the lone pair on the nitrogen and the lone pair in the carbene.

Changes in $R_{non-rot}$ are not as dramatic as for R_{rot} and do not vary much in the **1**, **2**, and **3** series. Other geometrical changes are worth noting: (a) the α = ∠NCN angle closes as the rotation proceeds to the TS, and (b) the nitrogen atom involved in the rotation pyramidalizes strongly.

Table 3 shows the computed thermodynamic activation parameters to rotation about the $C_{carbene}-N$ bond for species **1a**, **1b**, **2a**, **2b**, **3a**, and **3b**. These calculations include thermal corrections, which are calculated at the temperature the experiment was carried out (see below). As shown in Table 3 the

TABLE 3: Thermal Corrections ($T = 222.15$ K, $P = 1$ atm for All Species except 2a and 2b, with $T = 311.15$ K, $P = 1$ atm) to the Thermodynamic Activation Parameters in the Barriers to Rotation about the $C_{carbene}-N$ Bond for Species 1a, 2a, 3a, 1b, 2b, and 3b Using the B3LYP/6-31G* Model[a]

species	$\Delta G^{\ddagger}$	$\Delta H^{\ddagger}$	$\Delta S^{\ddagger}$	$\Delta G^{\ddagger}$(exp)
1a	81.0	81.2	0.9	
2a	104.5	104.7	0.7	
3a	97.0	97.6	2.7	
1b	45.0	42.6	−11.0	43.5[b]
2b	73.0	68.0	−16.1	64.0[c]
3b	62.0	57.9	−18.5	

[a] $\Delta G^{\ddagger}$ and $\Delta H^{\ddagger}$ are in kJ mol^{-1}, and $\Delta S^{\ddagger}$ is in J mol^{-1} K^{-1}. $\Delta G^{\ddagger}$(exp) is the experimental activation free energy (in kJ mol^{-1}) to rotation about the $C_{carbene}-N$ bond. [b] Dynamical ^{13}C NMR measure in **1b** with coalescence temperature $T_c = 222.15$ K and $P = 1$ atm. [c] **2b** with coalescence temperature $T_c = 311.15$ K and $P = 1$ atm.

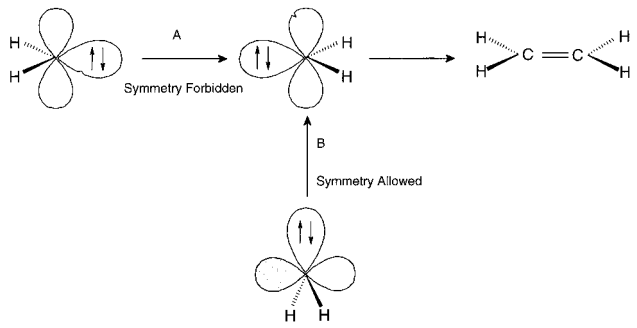

Figure 4. Least motion (A) and nonleast motion (B) pathways in the dimerization of two methylene molecules.

calculated barriers to rotation ($\Delta H^{\ddagger}$) are larger for the formamidinium ions **2a** and **2b** than for carbenes **1a** and **1b** and are larger for series **a** than for **b**. The activation free energies of rotation $\Delta G^{\ddagger}$ in **1b** and **2b** have been determined from dynamic ^1H NMR; coalescence temperatures are, respectively, −51 and 38 °C, and thermal corrections to the B3LYP/6-31G* calculated values were performed at these temperatures (and 1 atm of pressure), through frequency calculations at the stationary points for reactants and transition states using the B3LYP/6-31G* model. The frequencies in the thermal corrections were scaled by a factor of 0.9804 (at the B3LYP/6-31G* level).[42] Calculated $\Delta G^{\ddagger}$ values compare well with experiment for species **1b** and **2b**, the differences between theory and experiment being 1.5 and 9.0 kJ mol^{-1}, respectively. This agreement may hide significant problems, however, since **2a** probably exists largely as a lithium complex in THF solution. The calculated barrier for lithium complex **3b** is substantially higher than that for **1b** however, so it seems possible that rotation occurs via low concentrations of the free carbene. Also, we have reported[9] measurements for **1c** ($\Delta G^{\ddagger} = 53$ kJ mol^{-1}) and **2c** ($\Delta G^{\ddagger} = 55$ kJ mol^{-1}), and it is very hard to understand why changing Me into Pr^i should *increase* the barrier for the carbene but *lower* it for the formamidinium ion. At present, we believe that the experimental data for **1b** and **2b** is likely to be more representative than that for **1c** and **2c**, but more experimental work on these barriers is clearly required.

C.1. Dimerization of Diaminocarbene 1a. The dimerization of the simplest carbene, methylene, has been extensively examined theoretically following the original suggestion by Hoffmann et al.[22] that this reaction cannot proceed by a least motion pathway (A in Figure 4). Further theoretical studies (see ref 23 and references therein) showed that the triplet dimerization proceeds without a barrier by either the least motion (A) or the nonleast motion (B) pathway, and that the singlet

TABLE 4: Geometries of the Optimized Transition States (TS) for the Dimerization of 1a at Different Levels of Theory[a]

method/basis set	R_1	R_2	R_3	α	$\gamma(C_1)$	$\gamma(N_3)$	$\gamma(N_4)$	T
CAS(4,4)/6-31G*	2.091	1.355	1.368	111.1	24.3	2.6	12.0	39.4
CAS(4,4)/cc-pVDZ	2.086	1.360	1.366	111.1	23.8	7.0	11.9	45.6
MP2/6-31G*	2.057	1.357	1.369	110.9	24.8	2.6	12.6	37.0
MP2/cc-pVDZ	2.060	1.360	1.373	110.9	24.6	4.6	15.5	36.4
BPW91/6-31G*	2.211	1.359	1.369	111.6	25.3	2.0	11.8	25.4
BPW91/cc-pVDZ	2.176	1.360	1.368	111.8	24.5	3.4	12.6	28.0
B3LYP/6-31G*	2.095	1.357	1.367	111.6	23.7	2.9	12.0	32.7
B3LYP/cc-pVDZ	2.072	1.358	1.366	111.8	23.0	4.5	12.7	34.3

[a] All TS have C_2 symmetry (see Figure 5): $R_2 = R_4$, $R_3 = R_5$, $\alpha = \alpha'$; the pyramidalization angle is defined as $\gamma = 360 - (\beta_1 + \beta_2 + \beta_3)$ (see Figure 2); $\gamma(C_1) = \gamma(C_2)$, $\gamma(N_3) = \gamma(N_5)$, $\gamma(N_4) = \gamma(N_6)$. The torsional angle T is defined as $N_5C_2-C_1N_3$. Angles in degrees. Distances in Ångstrom.

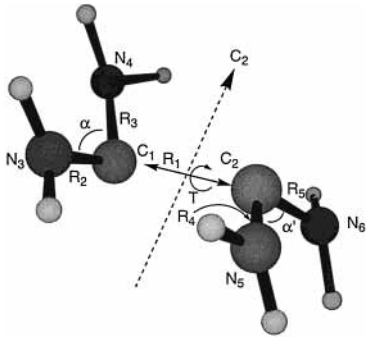

Figure 5. Transition state geometry in the dimerization of **1a**.

TABLE 5: Energy Differences (kJ mol^{-1}) in the Dimerization of 1a at Different Levels of Theory with the cc-pVDZ Basis Set[a]

method	ΔE(TS − R)	ΔE(TS − P)	ΔE(R − P)
CAS(4,4)	80.21	287.97	207.75
MP2	47.66	276.94	229.28
BPW91	35.24	224.95	189.71
B3LYP	46.11	227.61	181.50
QCISD(T)//MP2	48.33	251.08	202.75

[a] R, TS, and P stand for reactant (**1a**), transition state, and product, respectively. All calculations correspond to the species at $T = 0$ K without zero-point energy corrections.

dimerization by either pathway may lead to a Rydberg excited state of ethylene with the symmetry of the ground state. While the ground state in methylene is a triplet with ΔE(T−S) ≈ 40 kJ mol^{-1}, species **1a** and **1b** are singlets in the ground state with a ΔE(S−T) of 221 and 173 kJ mol^{-1} (B3LYP/cc-pVDZ model), respectively, so that one should not in principle expect any triplet intrusion in the dimerization process.[43]

One of the most striking features of **1b** is its slow dimerization at ambient temperatures. We have studied this dimerization in the range of temperatures from 0 to 40 °C, obtaining good second-order kinetics, but we now recognize that the rate of dimerization in THF solution is probably strongly dependent on lithium ion concentration, so that appropriate experimental data for comparison with calculated barriers is not available. To study theoretically the dimerization of the real carbene **1b**, we first simplified the molecule substituting the methyl groups for hydrogens and so started the calculations with **1a**: Reactant (R, C_{2v} symmetry), transitions states (TS), and products (P, D_2 symmetry tetrakis(amino)ethene) were optimized using different levels of theory. Table 4 and Figure 5 show the optimized TS geometries in the dimerization of **1a**. As this system is relatively small, one can use highly correlated wave functions for at least the single-point energy calculations. The full geometry optimization of R, TS, and P was carried out using complete active space self-consistent field theory with four electrons in four orbitals (CAS(4, 4)), second-order Møller−Plesset perturbation theory (MP2), and density functional theory with the BPW91 and B3LYP functionals. Single-point energy calculations at the QCISD(T) level of theory were performed with the MP2 optimized geometries. Figure 5 shows the labeling of the atoms in a general TS and the trans-bent conformation in the two diaminocarbenes. This conformation is similar to the one predicted by Hoffmann et al.[22] in the dimerization of methylene. In the preliminary calculations for the dimerization of **1a**, we found that the Hartree−Fock (HF) model shows a dipolar TS without symmetry, with $\delta^+(C_1)$ and $\delta^-(C_2)$ formal charges, and thus the TS geometry changes when including (nondynamic and dynamic) correlation energy: the symmetry of the TS augments from C_1 to C_2.[44] The C_2 axis of symmetry in the TS is in the plane of the paper in Figure 5 and bisects the C_1C_2 line. The higher symmetry provides a smaller dipole moment for the TS (from 0.96 D, B3LYP/cc-pVDZ, to 1.26 D, BPW91/cc-pVDZ). The most dramatic change with the inclusion of correlation energy stems from the pyramidalization on C_1, hence showing an important reorganization of the two diaminocarbene fragments when passing from C_1 to C_2 symmetry. As shown in Table 4, $\gamma(C_1) \sim 23-25°$ and the pyramidalization on nitrogens are within the values $\gamma(N_3) = 3-5°$ and $\gamma(N_4) = 13-16°$.

The product (P) in the dimerization of **1a** is tetrakis(amino)-ethene, which has D_2 symmetry. Since we are more concerned with the barriers to dimerization of **1a**, we shall only give the optimized geometrical parameters of P at the B3LYP/cc-pVDZ level. Using the same notation as in Figure 5: R(CC) = 1.355 Å, R(CN) = 1.421 Å, ∠NCN = 111.0°, and γ(N) = 26.4°.

Table 5 shows the ΔE(TS−R), ΔE(TS−P), and ΔE(R−P) energy differences in the dimerization of **1a** using different methods. The B3LYP barrier compares very well with the MP2 and the QCISD(T)//MP2 values, the difference being that such a method as QCISD(T) is computationally very demanding as compared to the B3LYP method. The CAS wave function also provides a good approximation to the QCISD(T)//MP2 value for the exothermicity.

To have a qualitative idea of the minimum-energy path (MEP) in the dimerization of **1a**, an intrinsic reaction coordinate (IRC) calculation[45] was performed following the reaction pathway from the TS to R-like and from the TS to P-like geometries using the BPW91/cc-pVDZ method, as shown in Figure 6. At this point it is necessary to emphasize that DFT, with the implementations (functionals) provided in the current codes, cannot describe even at a qualitative level such a simple process as the bond breaking in the following reaction: $H_2 \rightarrow H + H$.[46] It is important to emphasize that the DFT density is obtained from a set of orbitals in a monodeterminantal wave function.

The MEP in Figure 6 shows the high exothermicity and the relatively low barrier to dimerization in **1a**; the MEP was followed from $s = -4a_0$ (R-like) to $s = +4a_0$ (P-like) with a step of $0.2a_0$, corresponding to a total number of 40 points along the MEP without including the TS, which is given a value of $s = 0$.

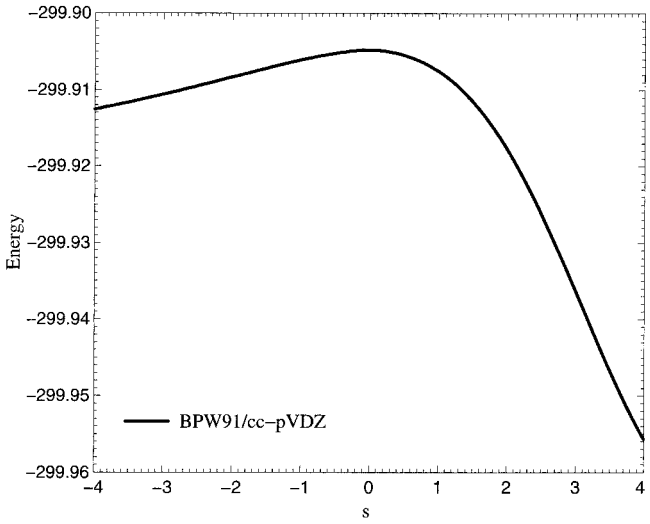

Figure 6. Minimum-energy path (MEP) for the dimerization of **1a** calculated at the BPW91/cc-pVDZ level of theory.

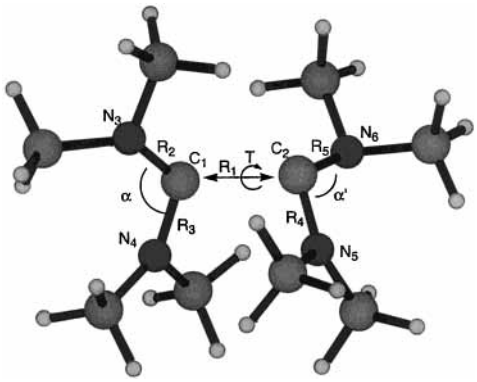

Figure 7. Transition state geometry in the dimerization of **1b**.

Thermal corrections to the barrier to dimerization in **1a** were performed at the B3LYP/6-31G* level; these results will be shown in due course for convenience when comparing the barriers with those in the dimerization of **1b**. Before proceeding to this discussion, it is worth noting that the nitrogen atoms in the TS for the dimerization of **1a** are pyramidalized anti to the forming C···C bond, leading to a relatively short contact between pairs of hydrogen atoms on the two fragments, which would develop into severe repulsion in the corresponding TS structure for **1b**. Several attempts were made to find alternative transition states in which the nitrogens were pyramidalized syn to the forming C···C bond, but no such stationary point could be found. We also searched without success for a TS in which the forming ethene fragment would be cis- rather than trans-bent.

C.2. Dimerization of Bis(dimethylamino)carbene 1b. Turning now to the dimerization of **1b**, we performed R, TS, and P geometry optimizations using the BPW91 and B3LYP functionals. TS geometry optimizations in the dimerization of **1b** using such methods as MP2 or QCISD(T) with the cc-pVDZ and larger basis sets become prohibitive. Therefore, DFT provides a very good alternative for the calculations of activation parameters in the dimerization of **1b**. Figure 7 and Table 6 show the geometry of the optimized TS for the dimerization of **1b**. As shown in Figure 7, the TS lacks any symmetry; this is to be contrasted with the dimerization of **1a** (see Figure 5). This lack of symmetry is reminiscent of the HF TS for **1a** but now persists even in calculations including correlation energy. The R_1 distances in the TS for the dimerizations of **1b** and **1a** differ by

TABLE 6: Optimized Transition State (TS) Geometries in the Dimerization of 1b Using the BPW91 and B3LYP Functionals[a]

method/basis set	R_1	R_2	R_3	R_4	R_5	α	α′
BPW91/6-31G*	2.267	1.369	1.367	1.370	1.430	117.5	111.6
BPW91/cc-pVDZ	2.252	1.370	1.369	1.372	1.431	117.5	111.8
B3LYP/6-31G*	2.140	1.366	1.363	1.367	1.437	116.7	111.1
B3LYP/cc-pVDZ	2.128	1.366	1.364	1.368	1.438	116.6	111.2

method/basis set	$\gamma(C_1)$	$\gamma(C_2)$	$\gamma(N_3)$	$\gamma(N_4)$	$\gamma(N_5)$	$\gamma(N_6)$	T
BPW91/6-31G*	20.0	36.0	2.1	0.5	0.6	21.4	106.5
BPW91/cc-pVDZ	20.1	36.1	2.1	0.6	0.5	21.7	106.3
B3LYP/6-31G*	18.1	35.2	2.7	0.7	0.5	24.0	111.8
B3LYP/cc-pVDZ	18.1	35.3	2.7	0.7	0.4	24.4	112.1

[a] All TS have C_1 symmetry (see Figure 7). The pyramidalization angle is defined as $\gamma(\text{atom}) = 360 - (\beta_1 + \beta_2 + \beta_3)$ (see Figure 2). The torsional angle T is defined as $N_5C_2-C_1N_3$. Distances in angstroms and angles in degrees.

∼0.05 Å, the former being larger; this difference can be attributed to the steric repulsion between the methyl groups in **1b**; this repulsion may also be the origin of the loss of symmetry $C_2 \rightarrow C_1$ when substituting the hydrogens by methyl groups in the TS. In the work of Hoffmann et al.[22] a C_2 TS region was also found for the singlet dimerization of CH_2. As observed in the bond distances (Table 6) one can distinguish a left-hand side carbene fragment (shorter R_2 and R_3 bond distances: ∼1.36−1.37 Å) from the right one, the latter having one larger R_5 bond distance (see Figure 7) with a value of 1.438 Å (B3LYP/cc-pVDZ). The R_4 bond distance (1.368 Å) in the right fragment is similar to the R_2, R_3 ones. $R_5 = C_2-N_6$ is precisely the bond to the strongly pyramidalized nitrogen N_6 as shown in Figure 7. In other words there is an evident charge transfer between the two carbon atoms in this TS, leading to a higher dipole moment (2.58 D at the B3LYP/cc-pVDZ level) as compared to the TS in the dimerization of **1a**. Here we should emphasize that the Hoffmann nonleast motion approach does suggest the possibility of one carbene acting as a nucleophile toward the other (and so becoming positively charged as it does), even though the calculations on dimerization of methylene itself and our calculations on **1a** do not support much charge separation in the TS. Note the pyramidalization of the $C_{carbene}$ in the dimerization of **1b**: Table 6 shows a clear difference between $\gamma(C_1)$ and $\gamma(C_2)$. The torsional angle T in Figures 5 and 7 is a measure of the trans-like or cis-like conformation in the TS geometry. Thus, a value of $T \sim 34°$ is found in the trans-conformation for the TS in the dimerization of **1a**; this value increases to $T \sim 112°$ for the TS in the dimerization of **1b** (Table 6); this difference shows the less clearly trans-bent conformation in the TS from Figure 7. The dramatic geometry changes shown in Figures 5 and 7 might have their origin in the presence of methyl groups. A possible explanation is that the electronic delocalization favoring quite a symmetric TS for the dimerization in **1a** no longer occurs for **1b** owing to the steric repulsion of the methyl groups. This repulsion provides a partial charge transfer from one carbon to another at the TS for the dimerization of **1b** (this would support the model disccused above, where one carbene acts as a nucleophile toward the other). This reasoning does not signify that we have located the only TS in the dimerization of **1b**, since other TS's might exist on the potential energy surface. Owing to the expense of the calculations, no other searches for TS's were carried out in the dimerization of **1b**. What can be asserted is that Hartree−Fock

TABLE 7: (a) Energy Barriers (kJ mol^{-1}) in the Dimerization of 1b Using the BPW91 and B3LYP Functionals;[a] (b) Thermal Corrections (B3LYP/6-31G* Model, $T = 293.15$ K, $P = 1$ atm) to the Activation Parameters in the Dimerization of 1a and 1b;[b] (c) Differences between the Energy Barriers in the Presence of Solvent (THF, Dielectric Constant $\epsilon = 7.58$ at 20 °C) and in the Gas Phase in the Dimerization of 1a and 1b: $\Delta(\Delta E) = \Delta E$(solvent) $- \Delta E$(gas), in kJ mol^{-1} [c]

(a)

method/basis set	ΔE(TS − R)	ΔE(TS − P)	ΔE(R − P)
BPW91/6-31G*	40.5	250.3	209.8
BPW91/cc-pVDZ	48.0	245.7	197.7
B3LYP/6-31G*	48.5	258.4	209.9
B3LYP/cc-pVDZ	56.9	253.6	196.7

(b)

dimerization	$\Delta G^{\ddagger}$	$\Delta H^{\ddagger}$	$\Delta S^{\ddagger}$	$\Delta E^{\ddagger}$
1a + **1a**	84.8	39.7	−154.1	42.1
1b + **1b**	102.0	48.8	−181.4	51.2

(c)

method/basis set	$\Delta(\Delta E)$ in **1a**	$\Delta(\Delta E)$ in **1b**
MP2/6-31G*	11.9	
MP2/cc-pVDZ	12.9	
BPW91/6-31G*	9.2	4.2
BPW91/cc-pVDZ	10.8	

[a] R, TS, and P stand for reactant, transition state, and product, respectively. [b] $\Delta G^{\ddagger}$, $\Delta H^{\ddagger}$, and $\Delta E^{\ddagger}$ in kJ mol^{-1} and $\Delta S^{\ddagger}$ in J mol^{-1} K^{-1}. [c] In the dimerization of **1a**, the reactant and transition state geometry was reoptimized in the presence of the solvent. In the dimerization of **1b**, the R and TS geometries were kept frozen (a single-point energy calculation was performed).

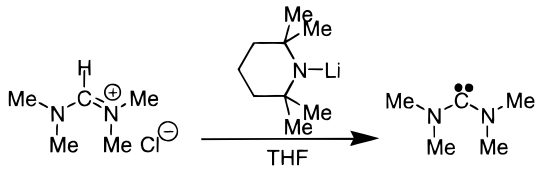

Figure 8. Experimental formation of **1b** from an amidinium salt in the presence of a lithum−piperidine base in THF-d_8 as a solvent.

TS's were first located for the dimerization of **1a** and **1b** and that inclusion of correlation energy via MP2 or DFT approaches led to a more symmetric TS for **1a** as compared to **1b**.

Table 7 shows the energy barriers in the dimerization of **1b**, computed with the BPW91 and B3LYP functionals. The current best estimate of experimental activation parameters (in THF-d_8 at 20 °C, probably involving lithium coordination) is $\Delta G^{\ddagger} = 89.9$ kJ mol^{-1}, $\Delta H^{\ddagger} = 75.2$ kJ mol^{-1}, $\Delta S^{\ddagger} = -49.7$ J mol^{-1} K^{-1}, and $\Delta E^{\ddagger} = 77.7$ kJ mol^{-1}. Experimentally the carbene **1b** is produced by deprotonation of the amidinium salt $[((CH_3)_2N)_2CH]^+Cl^-$ in the presence of a lithium−piperidine base as shown in Figure 8. It has been recently shown[20] that the complexation of carbenes with lithium, sodium, and even potassium species can occur and the effect of this on the carbene dimerization mechanism could be important. The calculated thermal corrections to the activation parameters for the dimerizations of **1a** and **1b** are shown in Table 7. The difference between the experimental and calculated activation parameters $\Delta G^{\ddagger}$, $\Delta H^{\ddagger}$, $\Delta S^{\ddagger}$, and $\Delta E^{\ddagger}$ are, respectively, 12 kJ mol^{-1}, 26 kJ mol^{-1}, 132 J mol^{-1} K^{-1}, and 16 kJ mol^{-1}. The thermal corrections for the dimerization of **1a** are introduced in Table 7 for comparative purposes: all activation parameters in the dimerization of **1b** are larger (in absolute value) as compared to **1a**. The experimental and computed $\Delta S^{\ddagger}$ values are negative because there are more degrees of freedom in 2*N* carbene molecules than in *N* transition structures ($S_1 > S_2^{\ddagger}$). Considering the carbene molecules to behave as an ideal gas (with weakly coupled degrees of freedom), one then has $S_{total} = S_{trans} + S_{rot} + S_{vib}$. Following the same order we have $S_{1,total} = 2(175 + 133 + 259)$ J mol^{-1} K^{-1} and $S_{2,total}^{\ddagger} = 166 + 110 + 98$ J mol^{-1} K^{-1} (B3LYP/6-31G* model). While the translational and rotational entropies are quite similar, the vibrational entropy difference is $S_{2,vib}^{\ddagger} - S_{1,vib} = -420$ J mol^{-1} K^{-1}.

It should be noted that there is a difference of 27 kJ mol^{-1} between the thermal corrected calculated activation energy $\Delta E^{\ddagger}$ (gas phase, Table 7) and the experimental one (liquid phase, from an Arrhenius plot of log *K* versus 1/*T*). The presence of Li^+ ions is probably the most important factor, but solvent effects might also be important. We performed several calculations using the Onsager model[47] in order to take into account the effect of the solvent THF-d_8 on the energy barrier to dimerization. These results are shown in Table 7 (bottom). For the dimerization of **1a** reactants and transition states were reoptimized in the presence of the solvent, while in the dimerization of **1b** the geometries of reactants and transition states were kept frozen. As is well-known, the Onsager model considers the solvent as a continuum medium of dielectric constant ϵ and the solute as an sphere of radius a_0, which can be calculated by computing the gas-phase molecular volume of the solute. Thus the difference between the experimental activation energy and the theoretical barrier (B3LYP/cc-pVDZ) for the dimerization of **1b** is 77.7 kJ mol^{-1} − 56.9 kJ mol^{-1} = 20.8 kJ mol^{-1}, but as shown in Table 7 the solvent correction only raises the barrier by ∼4 kJ mol^{-1} (BPW91/6-31G*).

D. Proton Affinities of Carbenes. The computation of proton affinities (PA) for carbenes **1a**, **1b**, **4c**, and $C(OH)_2$ at the B3LYP/6-31G* level of theory, including zero-point energy plus thermal corrections (298.15 K, 1 atm), provides the following values, respectively (kJ mol^{-1}): 1075.2, 1150.7, 1081.0, and 939.0. Dixon and Arduengo's calculation of the PA of the parent imidazol-2-ylidene **4c** gave a value of 1076.5 kJ mol^{-1} at the MP2 level,[25] almost identical to our value for **1a**, and which compares well with our calculation of 1081.0 kJ mol^{-1}. As expected from the inductive and polarizability effects of the methyl groups, **1b** is calculated to have a significantly higher PA. For comparison, we report the PA of $C(OH)_2$ above. Pliego and DeAlmeida[27] report a PA of 909 kJ mol^{-1} for $C(OH)_2$, using G2(MP2) theory.[48] Unfortunately, they do not specify which conformer was the global minimum for $C(OH)_2$ and $HC(OH)_2^+$ (protonated formic acid). We found that the global minimum in both molecules corresponds to the cis−trans- or "sickle"-conformer, in agreement with early MO calculations.[49] Protonated formic acid is an almost statistical mixture of the sickle- and W-conformers, according to NMR studies in superacid solution.[50] Pliego and DeAlmeida also report MP2/DZ//HF/DZ calculation of the PA for Ph_2C, 1151 kJ mol^{-1}, and fluorenylidene, 1140 kJ mol^{-1}. Two aryl substituents on the carbene center therefore produce almost the same PA as two dimethylamino groups, but two hydroxyl groups lead to a much lower PA. We feel that these trends are interesting but that the causes are by no means obvious, since both carbene and carbocation are clearly stabilized by π-electron donation (the latter to a larger extent),[26] while it might be expected that the carbene could also be stabilized by σ-electron withdrawal.

What can be asserted is that carbenes **1a**, **1b**, and **4c** are among the strongest neutral bases, in accord with our measurement of a pK_a of 24 in DMSO for **4b**. For comparison, the PA for one of the strongest amine bases, 1,8-bis(dimethylamino)-naphthalene (Proton Sponge) is calculated at the HF/6-31G*//

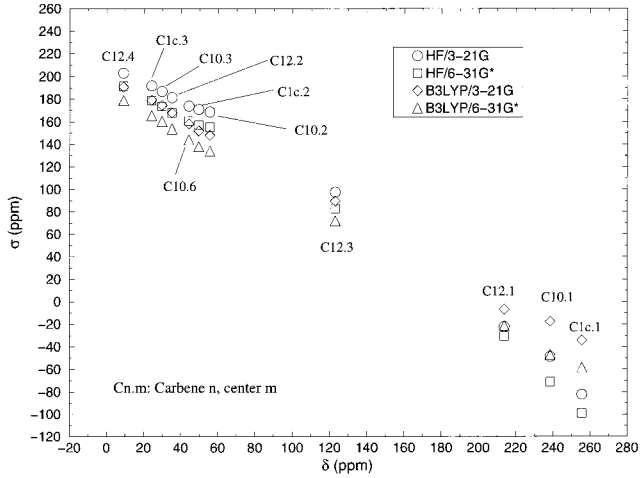

Figure 9. Plot of calculated ^{13}C isotropic shielding constants versus experimental chemical shifts for the carbenes **1c**, **10**, and **12** using the optimized geometries at the levels of theory shown in the small frame (top-right corner).

HF/6-31G level to be 1031 kJ mol^{-1},[51] while the experimental value is 1030 kJ mol^{-1}.[52]

E. ^{13}C NMR Chemical Shifts in Diaminocarbenes. This section comprises the analysis of experimental and computed ^{13}C NMR chemical shifts in the carbenes **1** and **9**−**15**. Among the different methods available in the suite of programs Gaussian94 for the calculation of NMR shielding tensors, the GIAO method of Ditchfield[35] has been efficiently implemented by Wolinski et al.[53] and gives reliable ^{13}C NMR chemical shifts. These calculations need reliable optimized geometries, and electron correlation energy should, in principle, be included. Calculations at the HF/6-31G*//B3LYP/6-31G* level have been recommended as the minimum model for NMR calculations, although larger basis sets with DFT are considered as preferable.[54] We have performed all chemical shifts calculations using the GIAO B3LYP/6-31G*//B3LYP/6-31G* model (however, we will briefly discuss the values of isotropic shielding constants as function of basis set size and inclusion of correlation energy). In a recent paper, Forsyth et al.[55] showed that this model gives reliable ^{13}C NMR chemical shifts (root-mean-square error ∼3 ppm) after empirical scaling on a set of 38 closed-shell stable organic molecules. Before proceeding to the geometry optimization calculations on the set of the above-mentioned carbenes, we checked the correlation between the computed isotropic ^{13}C magnetic shielding constants and the experimental ^{13}C NMR chemical shifts with three carbenes for which the X-ray structure is available: diaminocarbenes **1c**, **10**, and **12**, respectively. We found a better correlation between the experimental shifts and the optimized geometries (see Figure 9). Note the three clusters of points in Figure 9: The top-left cluster corresponds to the sp^3 $C_{carbene}$ nuclei. The center cluster corresponds to an sp^2 C center in Arduengo's carbene **10**, and finally the $C_{carbene}$ centers are gathered in the bottom-right cluster. As noted in this figure, for a given experimental chemical shift (*abscissa* axis) the isotropic shielding constants are ordered as $\sigma(\bigcirc) > \sigma(\square, \diamond) > \sigma(\triangle)$. For a given model, HF or B3LYP, augmenting of the basis set from 3-21G to 6-31G* gives $\sigma(\bigcirc) > \sigma(\square)$ and $\sigma(\diamond) > \sigma(\triangle)$, which is immediate from the former inequality. For a given basis set, inclusion of correlation energy (HF to B3LYP) gives $\sigma(\bigcirc) > \sigma(\diamond)$ and $\sigma(\square) > \sigma(\triangle)$. In other words, the effects of augmenting the basis set and including correlation energy are additive for the sp^2 and sp^3 C centers. Notwithstanding, these two effects are opposite for the $C_{carbene}$ centers: $\sigma(\bigcirc) > \sigma(\square)$ and $\sigma(\diamond) > \sigma(\triangle)$ as above when augmenting the basis set for a given model, but $\sigma(\bigcirc) < \sigma(\diamond)$ and $\sigma(\square) < \sigma(\triangle)$ when including correlation energy. These two effects offset one another, and hence the chemical shift on these centers will be quite sensitive to basis set size and the amount of correlation energy included.

SCHEME 1

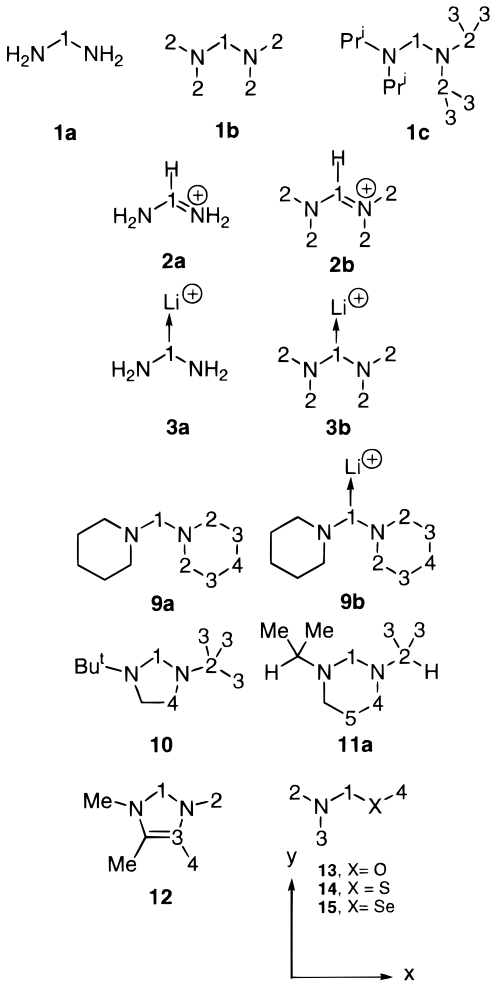

We now turn to the comparison between computed and experimental chemical shifts of the $C_{carbene}$ centers in carbenes **1** and **9**−**15**. The molecules shown in Scheme 1 are divided into three different groups: (i) **1a**, **1b**, **1c**, **9a**, **10**, **11a**, **11b**, and **12**; (ii) **2a**, **2b**, **3a**, and **3b**; (iii) **13**, **14**, and **15**; this grouping will become apparent below. Table 8 shows the calculated and experimental chemical shifts for group i diaminocarbenes. These shifts are correlated as depicted in Figure 10. Forsyth et al. scaled chemical shifts are overestimated by 10−20 ppm. The reason for this rather large deviation stems from the fact that no carbene molecules were included in their 38-compound list, the largest downfield chemical shift being that of C_2 in bicyclo-[2.2.1]heptan-2-one (δ_{exp} = 216.8 ppm). Our GIAO results show a deviation <8 ppm, which can be considered as acceptable given that the window on the ^{13}C shifts is 200−300 ppm. The $C_{carbene}$ chemical shift in **1b** is larger than the experimental one by 2 ppm. All other shifts are smaller by 2−8 ppm. Conformers **11a** and **11b** are calculated to almost equal in energy: E(**11a**) − E(**11b**) = 0.1 kJ mol^{-1} at the B3LYP/6-31G*//B3LYP/6-31G* level of theory. The preference for **11b** is rather surprising but is partially supported by the fact that the corresponding formamidinium ion and a potassium complex adopt this conformation.[20] The calculated shift for **11b** agrees better with experiment: δ_{calc}(**11a**) = 230.0 ppm, δ_{calc}(**11b**) = 232.7 ppm,

TABLE 8: Experimental and Calculated Chemical Shifts (ppm) for Group i Diaminocarbenes[a]

molecule	C center	δ_{exp}	δ_{GIAO}[b]	δ[c]
CH_2[d]	C		1281.1	1393.8
1a	C		226.0	242.5
1b	C_1	244.4	246.9	265.1
	C_2		43.4	44.6
1c	C_1	255.5	248.0	266.3
	C_2	49.6	51.7	53.5
	C_3	24.2	24.1	23.6
9a	C_1	236.8	254.3	273.1
	C_2	53.1	52.9	54.8
	C_3	27.4	28.3	28.2
	C_4	24.8	25.6	25.2
10	C_1	238.2	237.0	254.3
	C_2	55.7	55.5	57.6
	C_3	29.8	29.3	29.3
	C_4	44.4	45.6	46.8
11a	C_1	236.2, 219.1[e]	230.0	246.6
	C_2	58.2, 57.4	59.4	61.8
	C_3	21.4, 20.6	24.0	23.4
	C_4	36.9, 35.5	42.7	43.8
	C_5	22.4, 21.4	24.6	24.1
11b	C_1	236.2, 219.1	232.7	249.8
	C_2	58.2, 57.4	60.2	62.7
	C_3	21.4, 20.6	20.6	19.8
	C_4	36.9, 35.5	34.7	35.1
	C_5	22.4, 21.4	23.7	23.2
12	C_1	213.7	210.9	226.1
	C_2	35.2	36.2	36.7
	C_3	123.0	117.8	125.2
	C_4	9.0	10.8	9.2

[a] All calculations performed at the B3LYP/6-31G*//B3LYP/6-31G* level of theory. [b] The calculated chemical shifts refer to TMS: $\delta_{GIAO} = \sigma_{TMS} - \sigma$, with $\sigma_{TMS} = 189.7$ ppm at the B3LYP/6-31G*//B3LYP/6-31G* level of theory. [c] Using Forsyth's scaling equation $\delta = -1.084\sigma + 203.1$ (ppm) and the shielding constant σ calculated at the B3LYP/6-31G*//B3LYP/6-31G* level of theory. [d] GIAO calculation on the $^1A_1$ state. [e] The first and second chemical shift correspond, respectively, to measures under the following conditions: (1) KHMDS/THF, filtered, NMR in C_6D_6 and (2) LiTMP/toluene, NMR in C_6D_6 (shift moves to 236 on addition of 12-crown-4).

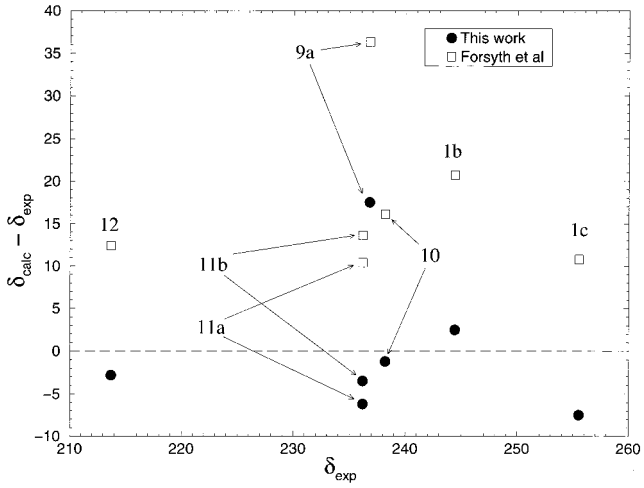

Figure 10. Plot of $\delta_{calc} - \delta_{exp}$ versus δ_{exp} for the $^{13}C_{carbene}$ nuclei in **1b**, **1c**, **9a**, **10**, **11a**, **11b**, and **12**. δ_{calc} correspond to GIAO B3LYP/6-31G*//B3LYP/6-31G* calculated chemical shifts relative to TMS.

and $\delta_{exp} = 236.2$ ppm. Table 8 gives two entries for the experimental shift in carbenes **11a** and **11b**. The first shift (δ_{exp}-(C_1) = 236.2 ppm) corresponds to a compound treated with KHMDS/THF and filtered, and the NMR signal measured in C_6D_6. The second shift ($\delta_{exp}(C_1) = 219.1$ ppm) corresponds to the limiting shift observed with excess LiHMDS in toluene-d_8 and is one example of the effect of lithium ion coordination.[20]

TABLE 9: Calculated Chemical Shifts (ppm) for Group ii Complexes 2a, 2b, 3a, 3b, and 9b[a]

complex	C center	δ_{exp}	δ_{GIAO}[b]	δ[c]
2a	C_1		144.4	154.0
2b	C_1		145.7	155.4
	C_2		41.6	42.6
3a	C_1		188.3	201.6
3b	C_1		202.9	217.4
	C_2		44.1	45.3
9b	C_1	236.8[d]	203.9	218.5
	C_2	53.1	55.8	58.0
	C_3	27.4	28.1	27.9
	C_4	24.8	23.7	23.2

[a] All calculations performed at the GIAO B3LYP/6-31G*//B3LYP/6-31G* level of theory. [b] The calculated chemical shifts refer to TMS: $\delta_{GIAO} = \sigma_{TMS} - \sigma$, with $\sigma_{TMS} = 189.7$ ppm at the B3LYP/6-31G*//B3LYP/6-31G* level of theory. [c] Using Forsyth's scaling equation $\delta = -1.084\sigma + 203.1$ (ppm) and the shielding constant σ calculated at the B3LYP/6-31G*//B3LYP/6-31G* level of theory. [d] These experimental chemical shifts are the same as those from carbene **9a** in Table 8. They are included here for comparative purposes.

TABLE 10: Calculated Chemical Shifts (ppm) for Group iii Carbenes 13, 14, and 15[a]

carbene	C center	δ_{exp}	δ_{GIAO}[b]	δ[c]
13	C_1	267[d]	263.9	283.5
	C_2		42.8	43.8
	C_3		27.7	27.5
	C_4		58.6	61.0
14	C_1	297[e]	305.8	328.9
	C_2		52.1	53.9
	C_3		39.3	40.0
	C_4		24.9	24.5
15	C_1		321.2	345.7
	C_2		52.1	53.9
	C_3		42.0	43.0
	C_4		20.4	19.5

[a] All calculations performed at the GIAO B3LYP/6-31G*//B3LYP/6-31G* level of theory. [b] The calculated chemical shifts refer to TMS: $\delta_{GIAO} = \sigma_{TMS} - \sigma$, with $\sigma_{TMS} = 189.7$ ppm at the B3LYP/6-31G*//B3LYP/6-31G* level of theory. [c] Using Forsyth's scaling equation $\delta = -1.084\sigma + 203.1$ (ppm) and the shielding constant σ calculated at the B3LYP/6-31G*//B3LYP/6-31G* level of theory. [d] Referred to carbene **7a**. [e] Referred to carbene **7b**.

TABLE 11: Diamagnetic (σ_d) and Paramagnetic (σ_p) Contributions (ppm) to the $^{13}C_{carbene}$ Magnetic Isotropic Shielding Constant (σ) in Group iii Carbenes 13, 14, and 15[a]

carbene	X	σ_d	σ_p	σ
13	O	250.3	−324.5	−74.2
14	S	257.2	−373.3	−116.1
15	Se	254.1	−385.6	−131.5

[a] All calculations performed at the GIAO B3LYP/6-31G*//B3LYP/6-31G* level of theory.

In the other case, e.g., **9a**, we cannot as yet disentangle the effects of lithium (or other metal) ion coordination. Thus, for **9a**, the Forsyth et al. scaling equation and our calculation overestimate the chemical shift on $C_{carbene}$ by 36 and 17 ppm, respectively. To study the effect of Li^+ complexation, a series of calculations were performed on the charged carbene-derived complexes $[(R_2N)_2C-M]^+$ with M = H, Li; these are the group ii compounds **2a**, **2b**, **3a**, **3b**, and **9b** shown in Scheme 1. Table 9 provides the calculated chemical shifts for these compounds. Comparison of the $C_{carbene}$ chemical shifts between **1a**, **2a** and **1b**, **2b** (see Tables 8 and 9) shows upfield shifts of 82 and 101 ppm, respectively, as expected for formamidinium ions. The effect of Li^+ complexation on diaminocarbenes **1a**, **1b**, and **9a** can be compared to their counterparts **1c**, **2c**, and **9b**, the

TABLE 12: Diamagnetic (σ_d) and Paramagnetic (σ_p) Shielding Tensors (ppm) on the $C_{carbene}$ Nucleus for CH_2 (Singlet $^1A_1$) and Carbenes 13, 14, and 15[a]

$$\sigma_p = \begin{vmatrix} \sigma_{xx} & \sigma_{yx} & \sigma_{zx} \\ \sigma_{xy} & \sigma_{yy} & \sigma_{zy} \\ \sigma_{xz} & \sigma_{yz} & \sigma_{zz} \end{vmatrix}$$

CH_2

$$\sigma_d = \begin{vmatrix} 255.1 & 0.0 & 0.0 \\ 0.0 & 247.1 & 0.0 \\ 0.0 & 0.0 & 247.9 \end{vmatrix} \qquad \sigma_p = \begin{vmatrix} -3461.6 & 0.0 & 0.0 \\ 0.0 & -537.6 & 0.0 \\ 0.0 & 0.0 & -46.3 \end{vmatrix}$$

13

$$\sigma_d = \begin{vmatrix} 269.9 & 3.7 & 0.0 \\ 0.0 & 254.7 & 0.0 \\ 0.0 & 0.0 & 226.3 \end{vmatrix} \qquad \sigma_p = \begin{vmatrix} -564.5 & -68.8 & 0.0 \\ -70.0 & -271.1 & 0.0 \\ 0.0 & 0.0 & -137.8 \end{vmatrix}$$

14

$$\sigma_d = \begin{vmatrix} 276.9 & 2.9 & 0.0 \\ 6.2 & 257.0 & 0.0 \\ 0.0 & 0.0 & 237.8 \end{vmatrix} \qquad \sigma_p = \begin{vmatrix} -681.1 & -38.5 & 0.0 \\ 7.7 & -313.5 & 0.0 \\ 0.0 & 0.0 & -125.3 \end{vmatrix}$$

15

$$\sigma_d = \begin{vmatrix} 275.3 & 5.5 & 0.0 \\ 7.3 & 254.1 & 0.0 \\ 0.0 & 0.0 & 232.8 \end{vmatrix} \qquad \sigma_p = \begin{vmatrix} -689.1 & -8.6 & 0.0 \\ 57.9 & -328.9 & 0.0 \\ 0.0 & 0.0 & -138.7 \end{vmatrix}$$

[a] All calculations performed at the GIAO B3LYP/6-31G*//B3LYP/6-31G* level of theory. The orientation of CH_2 is the same as that shown in Scheme 1 for **13**, **14**, and **15**.

differences in the shifts being 38, 44, and 50 ppm, respectively. This difference is about half that caused by protonation. Turning back to carbene **9a** and its Li^+ complex **9b**, Tables 8 and 9 show that the calculated chemical shifts δ(**9a**) = 254.3 ppm and δ(**9b**) = 203.9 ppm lie between the experimental value δ_{exp} = 236.8 ppm, the differences being $|\delta(\mathbf{9a}) - \delta_{exp}| = 17.5$ ppm and $|\delta(\mathbf{9b}) - \delta_{exp}| = 32.9$ ppm. The smaller shift in solution is readily attributed to a lower interaction with the metal ion, owing to its complexation by solvent molecules.

The aminooxy- and aminothiocarbenes **7a** and **7b**, respectively, were recently isolated in our laboratory.[18] To study the influence of the substituents on the chemical shift of the $C_{carbene}$ nucleus in amino−X−carbenes (X = O, S, and Se), compounds **7a** and **7b** were simplified to the group iii carbenes **13**, **14**, and **15**. Since oxygen and sulfur have a similar atomic electronic structure ([G]ns^2np,[4] G = He, n = 2 and G = Ne, n = 3), the aminoseleniumcarbene **15** (Se = [Ar]$3d^{10}4s^24p^4$) was also included for comparative purposes. The experimental and calculated chemical shifts for $C_{carbene}$ and the other C centers in group iii compounds are gathered in Table 10. The agreement for the aminooxycarbene **13** between the experimental and calculated $C_{carbene}$ shifts ($\Delta\delta$ = 3 ppm) is perhaps fortuitiously good, while that for aminothiocarbene **14** ($\Delta\delta$ = ∼9 ppm) is probably acceptable, in view of the unknown effects of the bulky substituents. As shown in Table 10, a difference of 30 ppm is found in the experimental chemical shift upon substitution of oxygen by sulfur, this difference being 42 ppm in the GIAO calculation. Substitution of sulfur by selenium gives a further 15 ppm downfield GIAO shift. To study the origin of the up- or downfield shifts upon substitution in carbenes **13**, **14**, and **15**, the $^{13}C_{carbene}$ GIAO magnetic isotropic shielding constant (σ) is split into the diamagnetic (σ_d) and paramagnetic (σ_p) contributions as shown in Table 11. Clearly, the difference is almost entirely due to the paramagnetic contribution (σ_d(**14**) − σ_d(**13**) ∼ 7 ppm and σ_p(**14**) − σ_p(**13**) ∼ 50 ppm when substituting oxygen by sulfur). Substitution of sulfur by selenium gives minor changes in the diamagnetic contribution (σ_d(**15**) − σ_d(**14**) ∼ −3 ppm) and a smaller change in the paramagnetic contribution (σ_p(**15**) − σ_p(**14**) ∼ 12 ppm). The dependence of the $C_{carbene}$ chemical shift on the substituents in carbenes **13**, **14**, and **15** can be explained in terms of the tensor components of the diamagnetic and paramagnetic shielding tensors, which are shown in Table 12. The orientation of the molecules is shown at the bottom of Scheme 1. As shown in Table 12 the diamagnetic components follow the order $\sigma_{d,xx} > \sigma_{d,yy} > \sigma_{d,zz}$ in all three carbenes (however, note that in $^1A_1$ CH_2, $\sigma_{d,yy} \sim \sigma_{d,zz}$). The paramagnetic contribution to the chemical shift in $^1A_1$ CH_2 is unusually large and negative[56] in the x-direction, and thus a chemical shift of ∼2300 ppm is predicted for this species.[56]

Arduengo et al. first reported the experimental chemical shielding tensor of a carbene (1,3,4,5-tetramethylimidazol-2-ylidene, carbene **12**) by means of solid-state NMR techniques,[29] the experimental absolute shielding tensors ($\sigma_{ii} = \sigma_{d,ii} + \sigma_{p,ii}$) on $C_{carbene}$ being σ_{xx} = −184(20) ppm, σ_{yy} = 9(18) ppm, and σ_{zz} = 104(15) ppm, the errors being given in parentheses. They also performed IGLO[57] and LORG[58] calculations at the Hartree−Fock and local density-functional theory (LDFT) levels of theory on $^1A_1$ CH_2, CF_2, carbene **12**, imidazol-2-ylidene, and the carbenium ions **12**·H^+ and imidazolium itself. Their IGLO and LORG $^{13}C_{carbene}$ chemical shifts calculated using the LDFT/TZVP model for carbene **12** are 188.8 and 196.8 ppm, respectively. It is clear from Table 8 that our GIAO B3LYP/6-31G*//B3LYP/6-31G* calculation (δ_{GIAO} = 210.9 ppm) is closer to the experimental value: δ_{exp} = 213.7 ppm in THF-d_8 and δ_{exp} = 209.6 ppm in the solid (using cross-polarization (CP), high-power proton decoupling, and magic angle spinning (MAS) techniques[29]).

Turning back to carbenes **13**, **14**, and **15**, it now becomes apparent from Table 12 the origin of the large paramagnetic contribution (σ_p) to the isotropic shielding constant: the large and negative $\sigma_{p,xx}$ components double the $\sigma_{p,yy}$ and $\sigma_{p,zz}$ counterparts. This effect is even more dramatic in $^1A_1$ CH_2 where the $\sigma_{p,xx}$ component is 6 and 75 times larger than the $\sigma_{p,yy}$ and $\sigma_{p,zz}$ ones, respectively. The explanation for such different σ_p (deshielding) components (especially in $\sigma_{p,xx}$) stems from the singlet−triplet gap in a given carbene, or in other words from the $n(a_1) \rightarrow \pi^*(b_1)$ transition. In $^1A_1$ CH_2, the virtual $2p_z$ or π^* orbital is practically empty (a CASSCF(6,6)/AUG-cc-pVTZ calculation on the singlet $^1A_1$ gives an occupancy n(n) = 1.90 and n(π^*) = 0.10, respectively), and in the presence of a magnetic field in the xy-plane, the angular momentum operator causes an electron in the lone pair n to jump into the empty π^* orbital (low-energy process), thus creating an electron "hole" in the plane of the molecule into which the electron may then jump back, permitting a facile circulation of electrons about the x- and y-axes and a paramagnetic (downfield) shift. When the out-of-plane π^* orbital is partially filled by σ-acceptor π-donor electron substituents (such as the ones in the carbenes studied in this work), the paramagnetic current is reduced depending on the electron density given into the π^* orbital. This reasoning explains why carbene **14** has a more negative and larger paramagnetic shielding constant as compared to carbene

13 since the difference between them is a sulfur and an oxygen atom attached to the $C_{carbene}$ center. As is well-known, the $C_{carbene}(\pi^*)-X(\pi)$ interaction is weaker in sulfur as compared to oxygen; hence, sulfur donates less π-electron density into the $\pi^*(C_{carbene})$ orbital and therefore $\sigma_{p,xx}$(**14**) $\ll \sigma_{p,xx}$(**13**), the difference $|\Delta\sigma_{p,xx}|$ being larger than 100 ppm. A similar but much smaller effect is found in the selenium-based carbene **15** as compared to **14**: $\sigma_{p,xx}$(**15**) $< \sigma_{p,xx}$(**14**), with $|\Delta\sigma_{p,xx}| \sim 8$ ppm. The paramagnetic current about the *y*-axis is also large and negative in the same order: $\sigma_{p,yy}$(**15**) $< \sigma_{p,yy}$(**14**) $< \sigma_{p,yy}$(**13**). Again the difference $|\Delta\sigma_{p,yy}| \sim 42$ ppm for **13** and **14** also indicates nonnegligible changes in the paramagnetic current about the *y*-axis. The paramagnetic contributions $\sigma_{p,zz}$ are less than half of $\sigma_{p,yy}$ and follow the order $\sigma_{p,zz}$(**15**) $\leq \sigma_{p,zz}$(**13**) $< \sigma_{p,zz}$(**14**) with similar values in all carbenes, the larger difference being only ~13 ppm ($\sigma_{p,zz}$(**14**) $- \sigma_{p,zz}$(**15**)).

As shown in Table 12, the antisymmetric components σ_{xy} and σ_{yx} in the diamagnetic and paramagnetic shielding tensors for carbenes **13**, **14**, and **15** do not vanish. These components contribute to second order in the magnetic field, producing negligible effects on spectra at achievable fields; they also contribute to the spin relaxation mechanisms.[59]

4. Conclusions

In this paper, we have tried to give some general insight into rotational and dimerization processes in diaminocarbenes **1a** and **1b**, as well as the influence of the substituents on the ^{13}C NMR chemical shifts for a set of diaminocarbenes and related species, and the dependence of these processes on complexation by protons and lithium ions.

Thermal-corrected computed energy barriers compare well with experiment for the rotation process in carbene **1b** and its protonated species **2b**. The difference between the theoretical and experimental energy barrier for the dimerization of **1b** should probably be mainly attributed to complexation of the free carbene with lithium ions in THF solution; solvent effects seem to be less important. The transition state in the dimerization of **1b** does not have any symmetry and shows a large charge-transfer effect between the carbon atoms forming the double bond. This structure is to be contrasted with the one in the dimerization of **1a**, the latter having C_2 symmetry and a lower dipole moment. Computed ^{13}C NMR chemical shifts for a series of diaminocarbenes and related species show satisfactory agreement with experimental measurements. The deviation of 2−8 ppm between theory and experiment in the chemical shifts at the $C_{carbene}$ nucleus may be attributed to the fact that the computed electronic density around this nucleus is highly dependent on the correlation energy and on the substituents in the amino centers. Magnetic shielding tensors $\boldsymbol{\sigma}$ have been calculated for amino−X−carbenes (X = O, S, Se), and it has been shown that the paramagnetic contribution plays an important role in the chemical shift changes upon substitution.

Acknowledgment. We thank Clare Webster for preliminary calculations of the rotational barriers. This work was supported by EPSRC Grant GR/K76160 (R.W.A.) and by the European Union TMR Grant ERBFMBICT97-2223 (J.M.O.). M.E.B. thanks EPSRC for a studentship.

References and Notes

(1) Arduengo, A. J., III; Harlow, R. L.; Kline, M. *J. Am. Chem. Soc.* **1991**, *113*, 361.

(2) For recent reviews, see: Herrmann, W. A.; Köcher, C. *Angew. Chem., Int. Ed. Engl.* **1997**, *36*, 2162.

(3) Arduengo, A. J., III; Krafczyk, R. *Chem. in unserer Zeit* **1998**, *32*, 6.

(4) Arduengo, A. J., III; Davidson, F.; Dias, H. V. R.; Goerlich, J. R.; Khasnis, D.; Marshall, W. J.; Prakasha, T. K. *J. Am. Chem. Soc.* **1997**, *119*, 12742.

(5) Arduengo, A. J., III; Dias, H. V. R.; Dixon, D. A.; Harlow, R. L.; Klooster, W. T.; Koetzle, T. F. *J. Am. Chem. Soc.* **1994**, *116*, 6812.

(6) Taton, T. A.; Chen, P. *Angew. Chem., Int. Ed. Engl.* **1996**, *35*, 1011.

(7) Arduengo, A. J., III; Goerlich, J. R.; Marshall, W. J. *J. Am. Chem. Soc.* **1995**, *117*, 11027.

(8) Denk, M. K.; Thadani, A.; Hatano, K.; Lough, A. J. *Angew. Chem., Int. Ed. Engl.* **1997**, *36*, 2607.

(9) Alder, R. W.; Allen, P. R.; Murray, M.; Orpen, A. G. *Angew. Chem., Int. Ed. Engl.* **1996**, *35*, 1121.

(10) Kuhn, N.; Kratz, T. *Synthesis* **1993**, 561.

(11) Enders, D.; Breuer, K.; Raabe, G.; Runsink, J.; Teles, J. H.; Melder, J.-P.; Ebel, K.; Brode, S. *Angew. Chem., Int. Ed. Engl.* **1995**, *34*, 1021. Enders, D.; Breuer, K.; Runsink, J.; Teles, J. H. *Liebigs Ann.* **1996**, 2019.

(12) Igau, A.; Grutzmacher, H.; Baceiredo, A.; Bertrand, G. *J. Am. Chem. Soc.* **1988**, *110*, 6463. Alcaraz, G.; Wecker, U.; Baceiredo, A.; Dahan, F.; Bertrand, G. *Angew. Chem., Int. Ed. Engl.* **1995**, *34*, 1246 and references therein.

(13) λ^3-Phosphinocarbenes such as **5** can also be regarded as λ^5-phosphaacetylenes, and related sulfur species are normally shown this way: Pötter, B.; Seppelt, K.; Simon, A.; Peters, E.-M.; Hettich, B. *J. Am. Chem. Soc.* **1985**, *107*, 980.

(14) Arduengo, A. J., III; Goerlich, J. R.; Marshall, W. J. *Leibigs Ann.* **1997**, 365.

(15) Breslow, R. *Chem. Ind.* **1957**, 893.

(16) Couture, P.; Terlouw, J. K.; Warkentin, J. *J. Am. Chem. Soc.* **1996**, *118*, 4214.

(17) Couture, P.; Warkentin, J. *Can. J. Chem.* **1997**, *75*, 1281.

(18) Alder, R. W.; Butts, C. P.; Orpen, A. G. *J. Am. Chem. Soc.* **1998**, *120*, 11526.

(19) Alder, R. W.; Blake, M. E. *Chem. Commun.* **1997**, 1513.

(20) Alder, R. W.; Blake, M. E.; Bortolotti, C.; Bufali, S.; Butts, C. P.; Lineham, E.; Oliva, J. M.; Orpen, A. G.; Quayle, M. J. *Chem. Commun.* **1999**, 241.

(21) Oliva, J. M. *Chem. Phys. Lett.* **1999**, *302*, 35.

(22) Hoffmann, R.; Gleiter, R.; Mallory, F. B. *J. Am. Chem. Soc.* **1970**, *92*, 1460.

(23) Ohta, K.; Davidson, E. R.; Morokuma, K. *J. Am. Chem. Soc.* **1985**, *107*, 3466.

(24) Alder, R. W.; Allen, P. R.; Williams, S. J. *J. Chem. Soc., Chem. Commun.* **1995**, 1267.

(25) Dixon, D. A.; Arduengo, A. J., III. *J. Phys. Chem.* **1991**, *95*, 4180.

(26) Hopkinson, A. C.; Lien, M. H. *Can. J. Chem.* **1985**, *63*, 3582. Hopkinson, A. C.; Lien, M. H. *Can. J. Chem.* **1989**, *67*, 991.

(27) Pliego, J. R.; DeAlmeida, W. B. *J. Chem. Soc., Faraday Trans.* **1997**, *93*, 1881.

(28) Muchall, H. M.; Werstiuk, N. H.; Choudhury, B. *Can. J. Chem.* **1998**, *76*, 221.

(29) Arduengo, A. J., III; Dixon, D. A.; Kumashiro, K. K.; Lee, C.; Power, W. P.; Zilm, K. W. *J. Am. Chem. Soc.* **1994**, *116*, 6361.

(30) West, R.; Buffy, J. J.; Haaf, M.; Müller, T.; Gehrhus, B.; Lappert, M. F.; Apeloig, Y. *J. Am. Chem. Soc.* **1998**, *120*, 1639.

(31) Van Geet, A. L. *Anal. Chem.* **1970**, *42*, 679. Kaplan, M. L.; Bovey, F. A.; Cheng, H. L. *Anal. Chem.* **1975**, *47*, 1703.

(32) Frisch, M. J.; Trucks, G. W.; Schlegel, H. B.; Gill, P. M. W.; Johnson, B. G.; Robb, M. A.; Cheeseman, J. R.; Keith, T.; Petersson, G. A.; Montgomery, J. A.; Raghavachari, K.; Al-Laham, M. A.; Zakrzewski, V. G.; Ortiz, J. V.; Foresman, J. B.; Cioslowski, J.; Stefanov, B. B.; Nanayakkara, A.; Challacombe, M.; Peng, C. Y.; Ayala, P. Y.; Chen, W.; Wong, M. W.; Andres, J. L.; Replogle, E. S.; Gomperts, R.; Martin, R. L.; Fox, D. J.; Binkley, J. S.; Defrees, D. J.; Baker, J.; Stewart, J. P.; Head-Gordon, M.; Gonzalez, C.; Pople, J. A. *GAUSSIAN94*; Gaussian, Inc.: Pittsburgh, PA, 1995.

(33) The smaller split valence shell 3-21G basis set was used in the GIAO calculations to study the effect of basis set size and correlation energy (see Figure 9).

(34) B3LYP: Becke's three parameter hybrid functional with the Lee−Yang−Parr correlation functional. BPW91: Becke's exchange functional with Perdew and Wang's correlation functional. Both models include local and nonlocal terms in the functionals.

(35) Ditchfield, R. *Mol. Phys.* **1974**, *27*, 789.

(36) We could not find any experimental data providing ideal C−N distances with respect to π-overlap and hybridization.

(37) Heinemann, C.; Thiel, W. *Chem. Phys. Lett.* **1994**, *217*, 11.

(38) The point-symmetry group for triplet diaminocarbene **1a** in Figures 1a,c is C_2. The C_{2v} nonplanar structure does not correspond to a global minimum at the levels of theory used in this work.

(39) McGibbon, G. A.; Kingsmill, C. A.; Terlouw, J. K. *Chem. Phys. Lett.* **1994**, *222*, 129.

(40) Feller, D.; Borden, W. T.; Davidson, E. R. *Chem. Phys. Lett.* **1980**, *71*, 22.
(41) Schmetzer, J.; Daub, J.; Fischer, P. *Angew. Chem., Int. Ed. Engl.* **1975**, *14*, 487.
(42) Wong, M. W. *Chem. Phys. Lett.* **1996**, *256*, 391.
(43) Although the S−T gaps in **1a** and **1b** are relatively large as compared to the T−S gap in CH_2, there is always the possibility that the triplet dimerization curve crosses the singlet curve before the TS is reached.
(44) We also located higher symmetry trans-bent C_{2h} TS's and found that they show a very small energy difference as compared to the C_2 TS's when including correlation energy. However, any C_{2h} TS is a second−order saddle point (two imaginary frequencies in the Hessian matrix).
(45) Fukui, K. *Acc. Chem. Res.* **1980**, *14*, 363.
(46) The functionals available in the literature and implemented into computer codes do not show one electron on each hydrogen as $R \rightarrow \infty$. A plot of energy versus R in H_2 does not show the proper convergence using the current implementations of DFT.
(47) Onsager, L. *J. Am. Chem. Soc.* **1936**, *58*, 1486.
(48) Curtiss, L. A.; Raghavachari, K.; Pople, J. A. *J. Chem. Phys.* **1993**, *98*, 1293.
(49) Ros, P. *J. Chem. Phys.* **1968**, *49*, 4902.
(50) Olah, G. A.; White, A. M. *J. Am. Chem. Soc.* **1967**, *89*, 3591. Hogeveen, H.; Bickel, A. F.; Hilbers, C. W.; Mackor, E. L.; Maclean, C. *Recl. Trav. Chim. Pays-Bas* **1967**, *86*, 687.
(51) Platts, J. A.; Howard, S. T.; Wozniak, K. *J. Org. Chem.* **1994**, *59*, 4647.
(52) Lau, Y. K.; Saluja, P. P. S.; Kebarle, P.; Alder, R. W. *J. Am. Chem. Soc.* **1978**, *100*, 7328.
(53) Wolinski, W.; Hinton, J. F.; Pulay, P. *J. Am. Chem. Soc.* **1990**, *112*, 8251.
(54) Cheeseman, J. R.; Trucks, G. W.; Keith, T. A.; Frisch, M. J. *J. Chem. Phys.* **1996**, *104*, 5497. Foresman, J. B.; Frisch, *Æ. Exploring Chemistry with Electronic Structure Methods*, 2nd ed.; Gaussian Inc.: Pittsburgh, PA, 1996; pp 21, 53, 104.
(55) Forsyth, D. A.; Sebag, A. B. *J. Am. Chem. Soc.* **1997**, *119*, 9483.
(56) van Wüllen, C.; Kutzelnigg, W. *J. Chem. Phys.* **1995**, *104*, 2330.
(57) Kutzelnigg, W. *Isr. J. Chem.* **1980**, *19*, 193.
(58) Hansen, A. E.; Bouman, T. D. *J. Chem. Phys.* **1985**, *82*, 5035.
(59) Spiess, H. W. *Nucl. Magn. Reson.: Basic Princ. Prog.* **1978**, *15*, 59.